PHYSICAL REVIEW B **81**, 140505(R) (2010)

Fermi-liquid behavior in an underdoped high-T_c superconductor

Suchitra E. Sebastian,[1,*] N. Harrison,[2,†] M. M. Altarawneh,[2] Ruixing Liang,[3,4] D. A. Bonn,[3,4] W. N. Hardy,[3,4] and G. G. Lonzarich[1]

[1]*Cavendish Laboratory, Cambridge University, J. J. Thomson Avenue, Cambridge CB3 OHE, United Kingdom*

[2]*National High Magnetic Field Laboratory, LANL, Los Alamos, New Mexico 87545, USA*

[3]*Department of Physics and Astronomy, University of British Columbia, Vancouver, Canada V6T 1Z4*

[4]*Canadian Institute for Advanced Research, Toronto, Canada M5G 1Z8*

(Received 30 December 2009; revised manuscript received 23 February 2010; published 21 April 2010)

We use magnetic quantum oscillations in the underdoped high T_c superconductor $YBa_2Cu_3O_{6+x}$ ($x \approx 0.56$) measured over a broad range of temperatures 100 mK$<T<$18 K to extract the form of the distribution function describing the low-lying quasiparticle excitations in high magnetic fields. Despite the proximity of $YBa_2Cu_3O_{6.56}$ to a Mott insulating state, various broken symmetry ground states and/or states with different quasiparticle statistics, we find that our experimental results can be understood in terms of quasiparticle excitations obeying Fermi-Dirac statistics as in the Landau-Fermi liquid theory.

DOI: 10.1103/PhysRevB.81.140505 PACS number(s): 74.72.−h, 74.25.Jb, 71.18.+y, 71.20.Ps

At the heart of our understanding of itinerant electron systems is Landau's Fermi-liquid theory in which gapless excitations on a Fermi surface in momentum space are governed by the Fermi-Dirac distribution.[1–4] One of the foremost examples of a breakdown of the Fermi-liquid paradigm occurs in fractional quantum Hall systems.[5] The validity of Landau-Fermi liquid theory could also be in question in other interacting systems[6] such as those at the border of electron localization.

The functional form of the Bose-Einstein distribution has been demonstrated in detail by means of a number of experiments including recent optical measurements in cold atomic gases.[7] Interestingly, however, it is not clear as to what extent of detail the precise form of the Fermi-Dirac distribution function—which is the basis of the theory of electron systems—has been measured.[4] In this Rapid Communication, we test the validity of Fermi-Dirac statistics governing the elementary excitations in one of the pre-eminent, most strongly correlated examples of a condensed matter system: the underdoped high T_c cuprates.[8] Quantum oscillations provide a unique means of accessing the statistical distribution governing quasiparticles of an interacting system. While other thermodynamic quantities such as heat capacity are useful in accessing the second moment (i.e., the variance) of the statistical distribution governing the system of interacting particles, we show here that quantum oscillation measurements access not only the second order moment but also the higher order moments and hence provide a more complete test of the applicability of the Landau-Fermi liquid description.

We measure magnetic quantum oscillations in $YBa_2Cu_3O_{6+x}$ ($x \approx 0.56$) (Refs. 9–14) over an extensive range of temperatures (100 mK$\leq T \leq$18 K) to obtain the temperature dependence of the oscillation amplitude $a(T)$. Quantum oscillations originate from changes in the occupancy of partially filled Landau levels at the Fermi energy ε_F as the magnetic induction **B** is varied, making their amplitude particularly sensitive to changes in the thermal distribution function $f(z)$ (where $z=[\varepsilon-\varepsilon_F]/k_BT$).[3] On increasing the temperature T, the broadened probability distribution $|f'(z)| = -\partial f/\partial z$ smears the phase of the quantum oscillations in energy ε (see Fig. 1), causing $a(T)$ to be reduced. The function $a(T)$ measures the Fourier transform of the statistical probability distribution $|f'(z)|$. We therefore use the inverse Fourier transform of the measured $a(T)$ to access the distribution of interacting quasiparticles in underdoped cuprates.

An accurate determination of $|f'(z)|$ requires $a(T)$ to be measured over a wide range of T. Here, we achieve a dynamic range of ~50 dB (see data in Fig. 2) by using the contactless conductivity technique (details described elsewhere[12,14,15]) in a motor generator-driven magnet delivering slowly swept magnetic fields to ~55 T in ^{4}He medium down to ~1 K and torque measurements in a continuous dc magnetic field reaching ~45 T in a dilution refrigerator. For

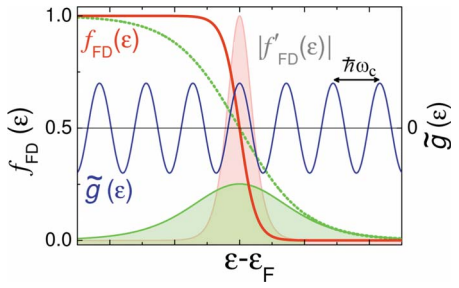

FIG. 1. (Color online) Considering the Fermi-Dirac distribution $f_{FD}=(1+e^z)^{-1}$ (where $z=[\varepsilon-\varepsilon_F]/k_BT$), the T-dependent step in occupation number (lines, dotted green for higher temperature) causes the oscillatory density of states $\tilde{g}=g_0e^{i2\pi\varepsilon/\hbar\omega_c}$ (assuming that g_0 is approximately constant on the scale of the cyclotron energy $\hbar\omega_c=\hbar eB/m^*$) shown by the blue (sinusoidal) line to be thermally smeared by the probability distribution $|f'_{FD}(z)|=1/(2+2\cosh z)$ (shaded regions). The consequent reduction in amplitude is equivalent to a Fourier transform of $|f'_{FD}(z)|$, yielding oscillations $\propto e^{i(2\pi F/B)}$ periodic in $1/B$ [F is the conventional quantum oscillation frequency (Ref. 3)] modulated by a T-dependent prefactor $a(T)=a_0\pi\eta/\sinh\pi\eta$ (where $\eta=2\pi k_BTm^*/e\hbar B$ and a_0 is a constant). The quantum oscillatory magnetization and resistivity can be expressed in terms of the above thermally averaged density of states, hence the same thermal amplitude factor $a(T)$.

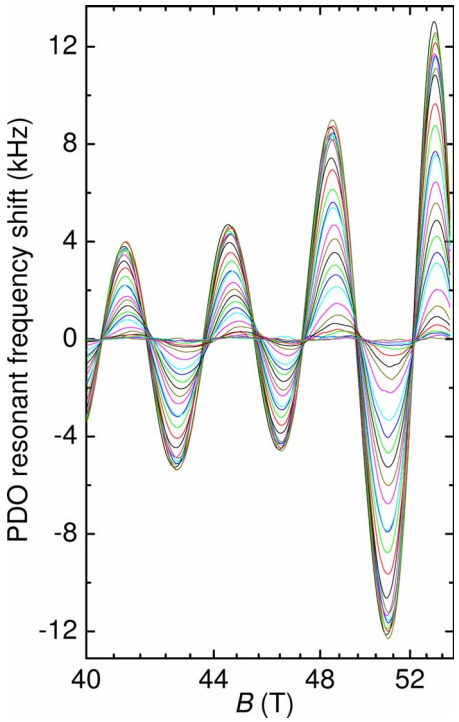

FIG. 2. (Color online) Quantum oscillations measured by the PDO contactless conductivity technique (Ref. 15) in $YBa_2Cu_3O_{6+x}$ with $x \approx 0.56$ (after background polynomial subtraction). This restricted interval in $B=|\mathbf{B}|$ furnishes a dynamic range of ~50 dB between $T=1$ and 18 K. The actual T values are provided in Fig. 3.

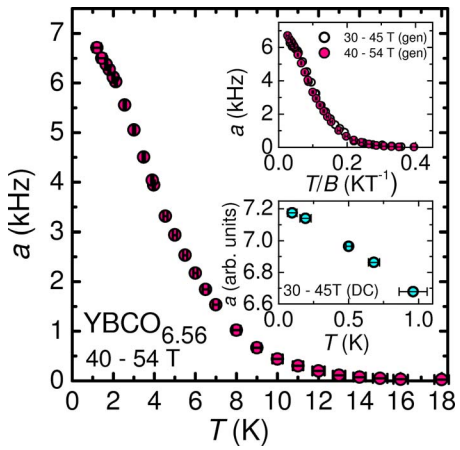

FIG. 3. (Color online) Quantum oscillation amplitude a versus T extracted by Fourier analysis of the data in Fig. 2 for $40 \leq B \leq 54$ T, corresponding to an average $B=45.96$ T. The upper inset shows the same data (filled circles) plotted versus T/B together with similar points extracted from the field interval $30 \leq B \leq 45$ T in which the amplitude has been normalized (open circles), matching the field range of the dc field torque measurements (lower inset). The close correspondence between field ranges implies that the dependence on T/B is independent of the interval in B within the resolution of the experiment, suggesting a magnetic field-independent m^*.

measurements in the motor generator-driven magnet, the uncertainty in T is minimized by ensuring that the sample is well coupled to the liquid cryogen (i.e., immersed in liquid ^{4}He), thereby minimizing heating due to irreversible field effects during the measurements for temperatures below 4.2 K. At these temperatures, the error in T is estimated from a comparison with dc field measurements and with the resistive crossover field providing an accurate secondary indication of T. At temperatures above 4.2 K, the error in T is estimated by repeating field sweeps at different vapor pressures of ^{4}He gas. Figure 2 shows the measured quantum oscillations in resonant frequency shift[15] after polynomial background subtraction at various temperatures; performing a Fourier transformation of the oscillations in $1/B$ using a Hann window yields $a(T)$ of the most prominent (α) oscillation shown in Fig. 3. Despite the close proximity of two other frequencies,[13] the temperature dependence of the α oscillation amplitude is unaffected since the other frequencies are much weaker than the α frequency, and the effective mass of all three frequencies has been measured to be nearly identical.[13]

To extend the range in T to lower values, we include low-temperature quantum oscillation data measured using magnetic torque in a dilution fridge in dc fields. The temperature error in these dilution fridge measurements could arise either from a nonlinear thermometer magnetoresistance or a drift in temperature stability during the magnetic field sweep. We calibrate the temperatures in a magnetic field by measuring the magnetoresistance between 11 and 45 T of the RuO_2 thermometer used for these measurements and collating them with the published values of magnetoresistance up to 8 T.[16] We find the magnetoresistance to behave very close to linearity for all $T \lesssim 1$ K, signaling that the chief error in T arises from thermal drift estimated from measured changes between rising and falling field. Although the dc fields extend only up to 45 T (lower inset of Fig. 3), the dependence of the amplitude on T/B is found to be independent of the interval in $1/B$ (upper inset of Fig. 3), enabling the contactless conductivity and torque data to be combined (upon amplitude renormalization at 1 K) in a plot of the oscillation amplitude versus the dimensionless parameter $\eta = 2\pi k_B T m^*/e\hbar B$ in Fig. 4(a).

The quasiparticle probability distribution is obtained by performing a Fourier transform of the quantum oscillation amplitude:

$$|f'(z)| = \left| a_0^{-1}(2\pi)^{-1} \int_{-\eta_{\lim}}^{\eta_{\lim}} e^{i\eta z} a(\eta) d\eta \right|. \quad (1)$$

Comparison with the model Fermi-Dirac distribution $|f'_{FD}(z)|$ involves two variable parameters: the effective mass m^* and amplitude normalization factor a_0. These are optimized by fitting the even partial moments

$$\mu_K = \int_{-z_{\lim}}^{z_{\lim}} z^K |f'(z)| dz \quad (2)$$

to those of the model probability distribution from the lowest-order moment upward. While the second moment μ_2 (i.e., variance) can be accessed by other thermodynamic experiments (e.g., heat capacity), a key advantage of quantum oscillation measurements is the ability to compare the entire

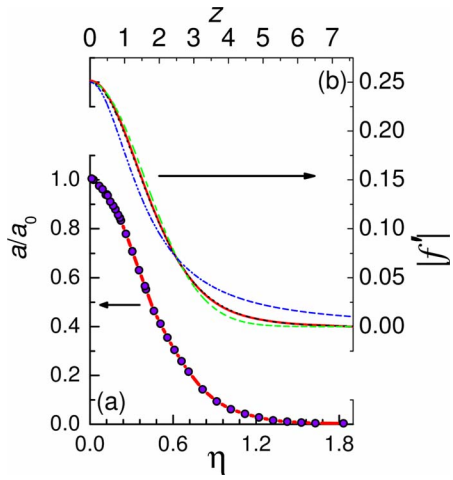

FIG. 4. (Color online) (a) Data (circles) from Fig. 3 plotted versus $\eta = 2\pi k_B T m^*/e\hbar B$, where $m^* = 1.676 m_e$. Data from the lower inset to Fig. 3 is included after amplitude normalization relative to the contactless conductivity data at $\eta \approx 0.15$. The line shows a linear interpolation. b Numerical Fourier transform of $a(\eta)$ in (a) (solid red line) obtained using Eq. (1), plotted over a restricted range of positive $z = \varepsilon / k_B T$, compared with the Fermi-Dirac (dotted black line), Gaussian (dashed green line) and Lorentzian (dot-dashed blue line) distributions.

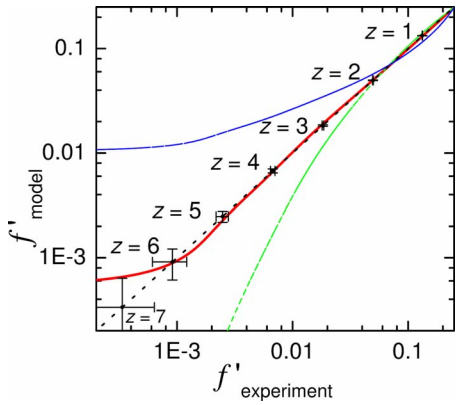

FIG. 5. (Color online) Comparison of the fitted probability distributions shown in Fig. 4 with that obtained from experiment. The Fermi-Dirac (solid red line), Gaussian (dashed green line) and Lorentzian (dot-dashed blue line) probability distributions are shown on the y axis as a function of the experimentally obtained probability distribution $|f'(z)|$ on the x axis. The + symbols locate integer values of z (the black dotted line is a guide to the eye), with the error bars indicating the extent to which experimental uncertainties (chiefly associated with the sample temperature) can cause $|f'(z)|$ to depart from $|f'_{FD}(z)|$.

hierarchy of moments with probability distribution models. The chief experimental limitation of quantum oscillation measurements is the breadth of the temperature range over which oscillations are measured. To perform the Fourier transform, evenly spaced points are required in $\pm\eta$. These are obtained by symmetrizing the data in Fig. 4(a) with respect to $T=0$ and making a linear interpolation (in the range $-\eta_{lim} < \eta_m < \eta_{lim} \approx 1.8$). The data are further padded with zeroes to yield a Fourier transform with points finely spaced in z. The combined effects of the finite range, spacing between data points and experimental uncertainty in Fig. 3 restrict the range in z to $-z_{lim} < z < z_{lim} \approx 7.5$, hence the comparison of "partial" moments in Table I and Eq. (2).

On adopting this procedure of multiple moment comparison for $-z_{lim} < z < z_{lim}$, we find optimized values of a_0 and $m^* = 1.676 \pm 0.001 m_e$ (where m_e is the free electron mass), for which the second (variance) and fourth (kurtosis) moments of the experimentally obtained probability distribution coincides to 4 and 3 significant digits with the Fermi-Dirac probability distribution, respectively. Good agreement continues to be found with the higher order moments, which we list in Table I up to μ_{10}. In Fig. 5 we compare the Fermi-Dirac distribution and the illustrative Gaussian and Lorentzian probability distributions against that obtained experimentally. This exercise demonstrates the importance of a wide temperature range in testing the goodness of fit of a probability distribution model—we see that the deviation from the Gaussian and Lorentzian models only appears above $z=2$. The deviation from an ideal Fermi-Dirac distribution occurs only above $z=6$ but falls within the experimental uncertainty. We note that a more limited set of data than we present here would not be able to distinguish between these alternative distribution functions were there to be increased scatter and/or a limited range in T, such as in Ref. 11.

Our study therefore indicates a high degree of correspondence between the elementary excitations in underdoped $YBa_2Cu_3O_{6+x}$ ($x \approx 0.56$) and those of fermionic quasiparticles governed by a Fermi-Dirac distribution. Hence, long-lived robust fermionic quasiparticles exist over a broad range of temperatures (100 mK $< T <$ 18 K). At first glance one may find this result surprising, especially in a system such as underdoped $YBa_2Cu_3O_{6+x}$ which is close to the Mott insulating state. We relook at whether we indeed have reason to find this result unexpected and investigate possible reasons why

TABLE I. Evaluation of the lowest even moments. The first row contains the lowest even moments of the Fermi-Dirac probability (corresponding to $z_{lim}=\infty$). The second row contains the corresponding partial moments of the Fermi-Dirac probability distribution using $z_{lim} = 7.5$ identical to the experimental data limits for purposes of comparison, and the third row contains the partial moments evaluated for the probability distribution extracted from the experimental data also using $z_{lim}=7.5$. Very good agreement is seen.

Moment μ_K	μ_2 variance	μ_4 kurtosis	μ_6	μ_8	μ_{10}
$\lvert f'_{FD}\rvert$ $(\pm\infty)$	3.2899	45.458	1419	8.03×10^4	7.25×10^6
$\lvert f'_{FD}\rvert$ $(\pm z_{lim})$	3.2089	39.123	875	2.70×10^4	9.94×10^5
$\lvert f'_{exp}\rvert$ $(\pm z_{lim})$	3.2085	39.128	873	2.65×10^4	9.49×10^5

Landau-Fermi liquid behavior prevails. We consider alternative scenarios that may be applicable to the ground state of underdoped $YBa_2Cu_3O_{6+x}$ and investigate whether they would be consistent with our experimental observation of Fermi-Dirac statistics. In addition to non-Fermi-Dirac statistics, the temperature dependence of the oscillation amplitude could deviate from that shown in Fig. 1 due to a nonconstant value of g_0 (as defined in Fig. 1 caption). An energy gap in the electronic structure near the Fermi energy of magnitude comparable to $\hbar\omega_c$ could yield a nonconstant value of g_0, such as in the case of symmetry-breaking ground states (e.g., density wave ordered states with Fermi surface reconstruction due to translational symmetry breaking and the superconducting vortex liquid). Any additional temperature dependence of the amplitude arising from these effects, however, appears not to be large enough to lead to a detectable deviation in our experiment from the temperature-dependent amplitude expected from Fermi-Dirac statistics.

Various other models would not be expected to lead to Fermi-Dirac statistics—a notable example being fractional quantum Hall effect in very high magnetic fields. In the case of underdoped $YBa_2Cu_3O_{6+x}$, models yielding oscillations unrelated to Landau quantization (e.g., Ref. 17) would not be expected to result in a temperature-dependent oscillation amplitude that agrees with Fermi-Dirac statistics and are therefore inconsistent with our experimental findings. To consider the applicability of various other non-Fermi-liquid models proposed for $YBa_2Cu_3O_{6+x}$ (e.g., Ref. 8), theoretical predictions are required for the energy scale at which a deviation from Fermi-Dirac statistics is expected. Such ground states could potentially go undetected in the current study if the deviation from Fermi-Dirac statistics takes place over an energy scale lower than that $\sim$100 mK of the lowest accessed temperature or for a different section of Fermi surface. Similar considerations may apply to the superconducting vortex liquid ground state in which regime the current experiments are performed. It will be of interest to determine conditions under which a breakdown of Fermi-Dirac statistics could occur for this ground state.

This work was supported by the U.S. Department of Energy, Office of Basic Energy Sciences, the NSF, Division of Materials Science and Engineering, the State of Florida, the Royal Society, and Trinity College (University of Cambridge).

*suchitra@phy.cam.ac.uk

†nharrison@lanl.gov

[1] L. D. Landau, Zh. Eksp. Teor. Fiz. **30**, 1058 (1956).

[2] P. Nozières, *Theory of Interacting Fermi Systems: Frontiers in Physics Series 19*, (Benjamin, New York, 1964).

[3] D. Shoenberg, *Magnetic Oscillations in Metals* (Cambridge University Press, Cambridge, 1984).

[4] N. W. Ashcroft and N. D. Mermin, *Solid State Physics: Problems and Solutions* (Brooks Cole, Belmont, MA, 1976).

[5] J. K. Jain and P. W. Anderson, Proc. Natl. Acad. Sci. U.S.A. **106**, 9131 (2009).

[6] A. Wasserman, M. Springford, and F. Han, J. Phys.: Condens. Matter **3**, 5335 (1991); A. C. Hewson, *The Kondo Problem to Heavy Fermions* (Cambridge University Press, Cambridge, 1997); P. Fazekas, *Lecture Notes on Electron Correlation and Magnetism*, Series in Modern Condensed Matter Physics 5 (World Scientific, Singapore, 1999).

[7] J. F. Annett, *Superconductivity, Superfluids, and Condensates* (Oxford University Press, New York, 2004).

[8] P. W. Anderson, P. A. Lee, M. Randeria, T. M. Rice, N. Trivedi, and F. C. Zhang, J. Phys.: Condens. Matter **16**, R755 (2004); P. A. Lee, N. Nagaosa, and X.-G. Wen, Rev. Mod. Phys. **78**, 17 (2006); C. M. Varma and L. Zhu, Phys. Rev. Lett. **98**, 177004 (2007).

[9] R. Liang, D. A. Bonn, and W. N. Hardy, Phys. Rev. B **73**, 180505(R) (2006).

[10] N. Doiron-Leyraud, C. Proust, D. LeBoeuf, J. Levallois, J.-B. Bonnemaison, R. Liang, D. A. Bonn, W. N. Hardy, and L. Taillefer, Nature (London) **447**, 565 (2007).

[11] C. Jaudet, D. Vignolles, A. Audouard, J. Levallois, D. LeBoeuf, N. Doiron-Leyraud, B. Vignolle, M. Nardone, A. Zitouni, R. Liang, D. A. Bonn, W. N. Hardy, L. Taillefer, and C. Proust, Phys. Rev. Lett. **100**, 187005 (2008).

[12] S. E. Sebastian, N. Harrison, M. M. Altarawneh, C. H. Mielke, R. Liang, D. A. Bonn, W. N. Hardy, and G. G. Lonzarich, Proc. Natl. Acad. Sci. U.S.A. **107**, 6175 (2010).

[13] S. E. Sebastian, N. Harrison, P. A. Goddard, M. M. Altarawneh, C. H. Mielke, R. Liang, D. A. Bonn, W. N. Hardy, O. K. Andersen, and G. G. Lonzarich, arXiv:1001.5015 (unpublished).

[14] S. E. Sebastian, N. Harrison, E. Palm, T. P. Murphy, C. H. Mielke, R. Liang, D. A. Bonn, W. N. Hardy, and G. G. Lonzarich, Nature (London) **454**, 200 (2008).

[15] M. M. Altarawneh, C. H. Mielke, and J. S. Brooks, Rev. Sci. Instrum. **80**, 066104 (2009).

[16] M. Watanabe, M. Morishita, and Y. Ootuka, Cryogenics **41**, 143 (2001).

[17] A. S. Alexandrov, J. Phys.: Condens. Matter **20**, 192202 (2008).